Electronic Supplementary Material (ESI)

A miniprotein receptor electrochemical biosensor chip based on quantum dot

Yunong Zhao,†[a] Juan Han,†[b] Jing Huang,[a] Qing Huang,[a] Yanbing Tao,[a] Ruiqin Gu,[a] Hua-Yao Li,[a] Yang Zhang,[c,d] Houjin Zhang,*[b] and Huan Liu *[a]

[a] *School of Integrated Circuits, Wuhan National Laboratory for Optoelectronics, Optics Valley Laboratory, Huazhong University of Science and Technology, Wuhan 430074, Hubei, China*

[b] *Department of Biotechnology, College of Life Science and Technology, MOE Key Laboratory of Molecular Biophysics, Huazhong University of Science and Technology, Wuhan 430074, Hubei, China*

[c] *Key Laboratory of Semiconductor Materials Science, Institute of Semiconductors, Chinese Academy of Sciences, Beijing 100083, China*

[d] *College of Materials Science and Opto-Electronic Technology, University of Chinese Academy of Sciences, Beijing 100049, China*

*Corresponding author: Houjin Zhang (hjzhang@hust.edu.cn); Huan Liu (huan@mail.hust.edu.cn)

† These authors contributed equally: Yunong Zhao, Juan Han

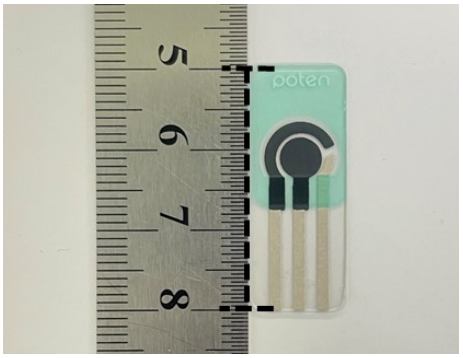

Fig. S1. The dimension of the electrochemical planar three-electrode.

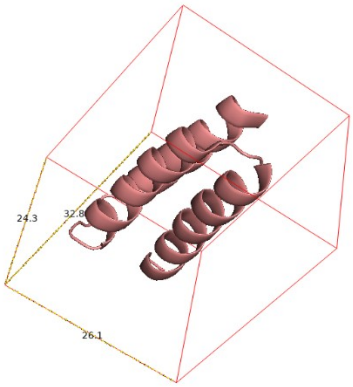

Fig. S2. Schematic diagram of molecule structure for LCB.

Pb element and Sulfur (S) element of CQDs were evenly distributed in the modification layer (**Fig. S3**). The unnatural receptor LCB was immobilized on the modification layer, and the surface shows the typical features of an undulating wavy structure (**Fig. S4**). The existence of the nitrogen (N) element indicated that LCB was efficiently modified on the CQDs modification layer, as N element is not present in the modification layer (**Fig. S5**).

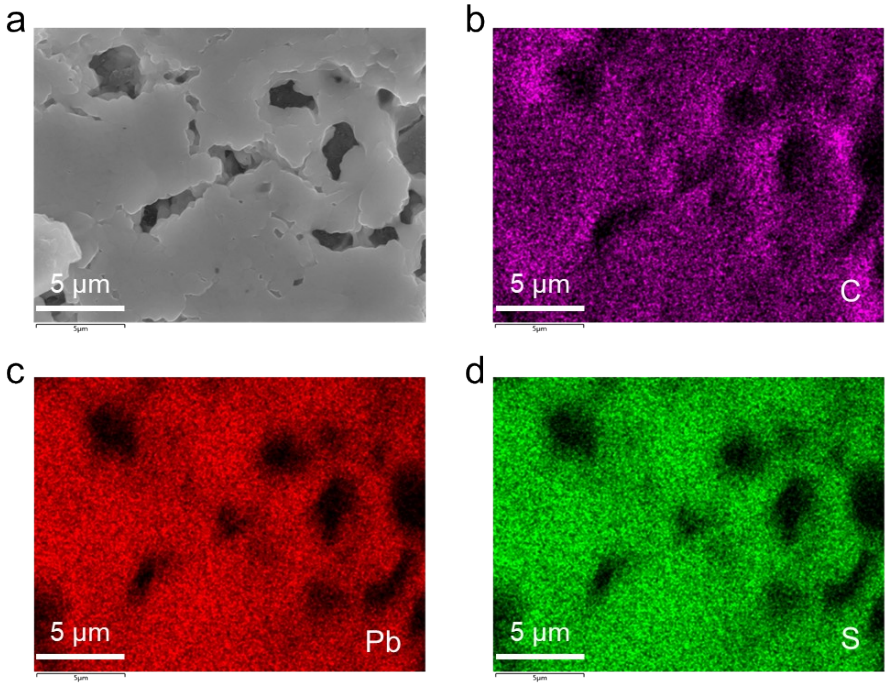

Fig. S3. (a) SEM image of CQDs film without LCB immobilization on the WE. (b-d) The EDS spectra of CQDs modification layer on the WE.

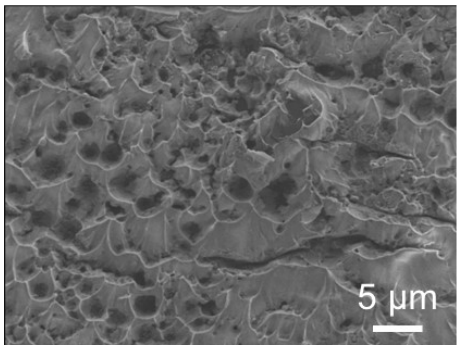

Fig. S4. SEM image of CQDs film with LCB immobilization on the WE.

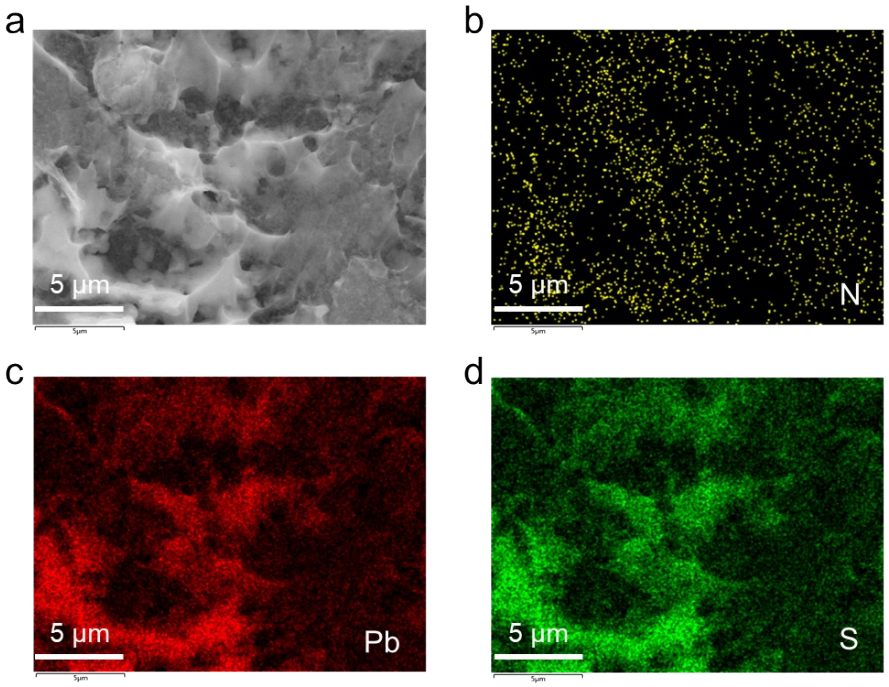

Fig. S5. (a) SEM image of CQDs film with LCB immobilization on the WE. (b-d) The EDS spectra of CQDs/LCB modification layer on the WE.

AFM characterizations further revealed the LCB immobilization increased the root mean square (RMS) roughness of CQDs modification layer, where the RMS roughness increased from 17.8 nm to 45.0 nm (within a 4 μm^2 area) (**Fig. S6**). After the coating by BSA, the film RMS roughness decreased to 18.7 nm, suggesting a good blocking effect at the non-specific binding sites (**Fig. S7**).

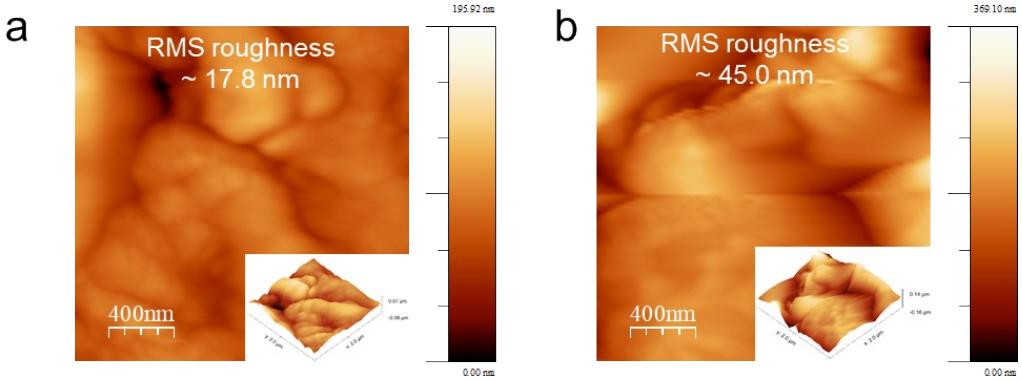

Fig. S6. (a) 3D AFM image of CQDs film without LCB immobilization. (b) SEM image of CQDs film with LCB immobilization on the WE.

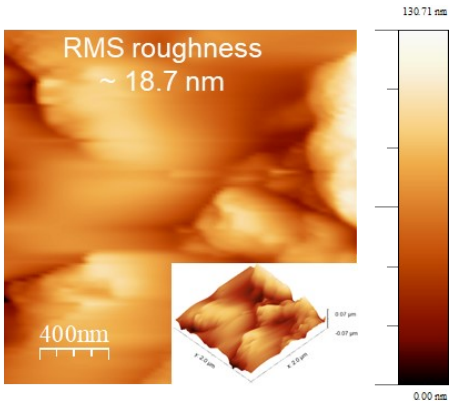

Fig. S7. 3D AFM image of CQDs/LCB film with BSA blocking.

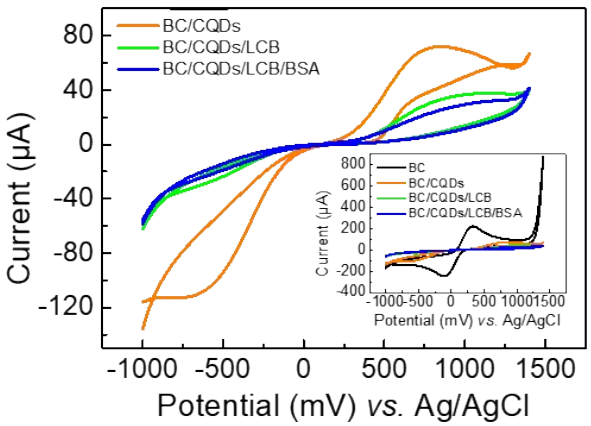

Fig. S8. CV characterizations of bare carbon electrode (BC), BC/CQDs, BC/CQDs/LCB, BC/CQDs/LCB/BSA electrode samples.

The tendency in peak current of CV curves was in accordance with DPV testing results. In addition, electrochemical impedance spectroscopy (EIS) could reveal the quantitative parameters of the equivalent circuit model and analyze the electrochemical system (**Fig. S9**). The current intensity was influenced by R_{ct} and Q, which indicates the capacitance of the electric double layer and the charge transfer resistance. CQDs modification layer caused a minute increase in R_{ct} value since the dangling bonds around CQDs result in poor conductivity (**Fig. S10**). For the electric double layer, the CQDs modification layer led to decreased Q value. Owing to the insulating properties of the unnatural receptor LCB and BSA, R_{ct} value increased gradually along the successive coating procedures. The BC/CQDs/LCB/BSA electrode had a relatively smaller R_{ct} value and higher Q value among the four electrode samples.

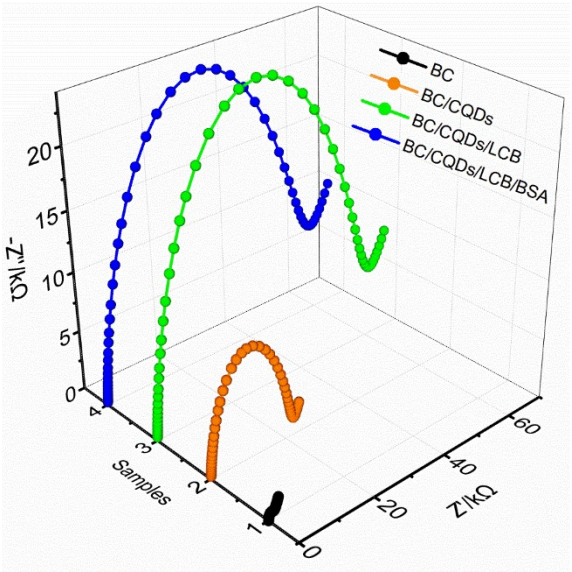

Fig. S9. EIS characterizations of bare carbon electrode (BC), BC/CQDs, BC/CQDs/LCB, BC/CQDs/LCB/BSA electrode samples.

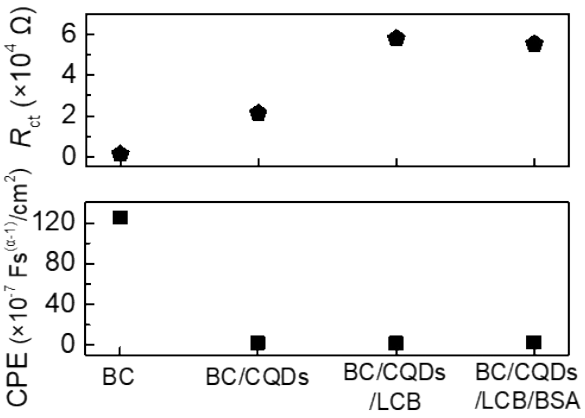

Fig. S10. R_{ct} and Q values for bare carbon electrode (BC), BC/CQDs, BC/CQDs/LCB, BC/CQDs/LCB/BSA electrode samples.

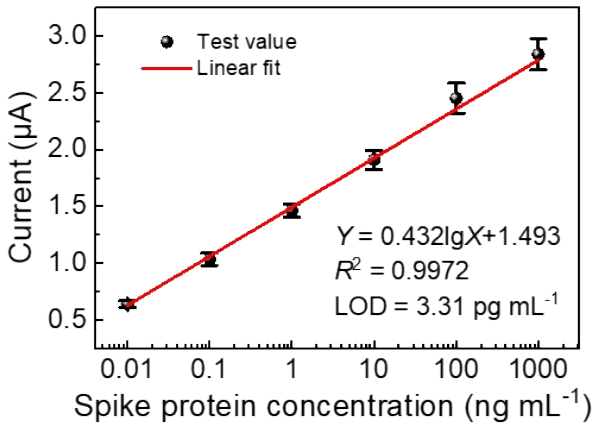

Fig. S11. The peak current values corresponding to increasing spike protein concentrations.

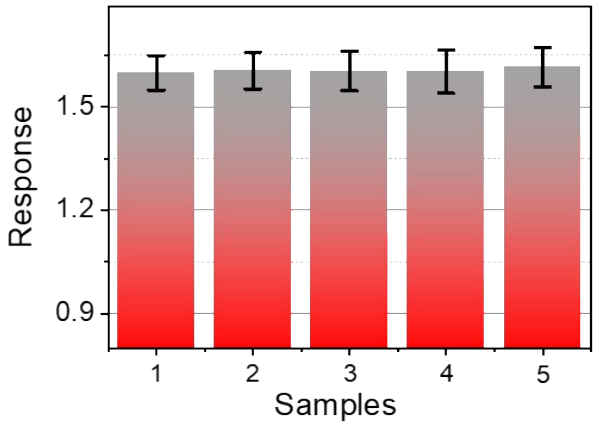

Fig. S12. Reproducibility analysis of the unnatural receptor-based biosensors.

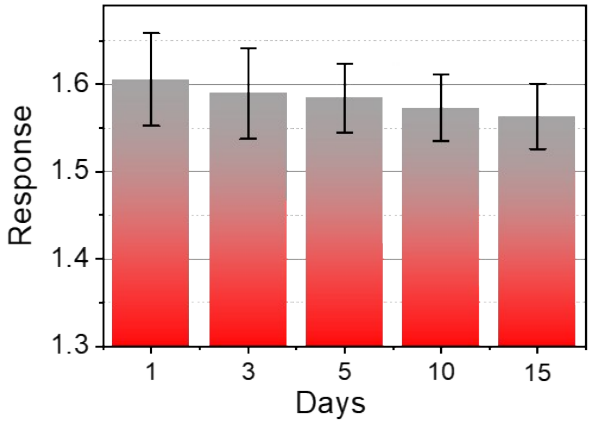

Fig. S13. Stability of the unnatural receptor-based biosensors.

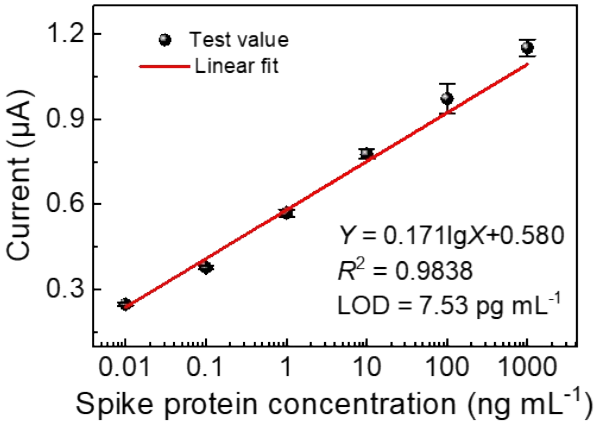

Fig. S14. The peak current corresponding to increasing spike protein concentrations for BC/CQDs/Antibody/BSA electrode.

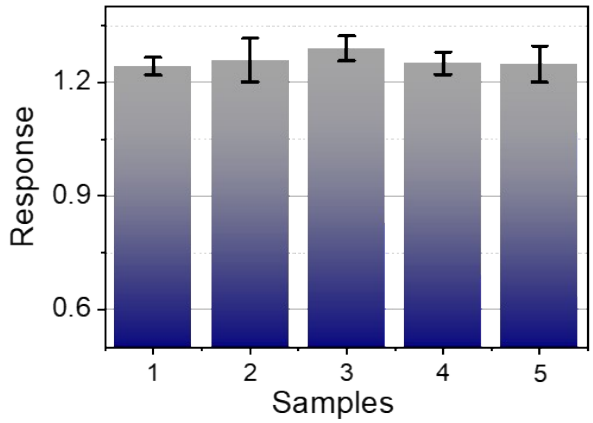

Fig. S15. Reproducibility analysis of the antibody-based biosensors.

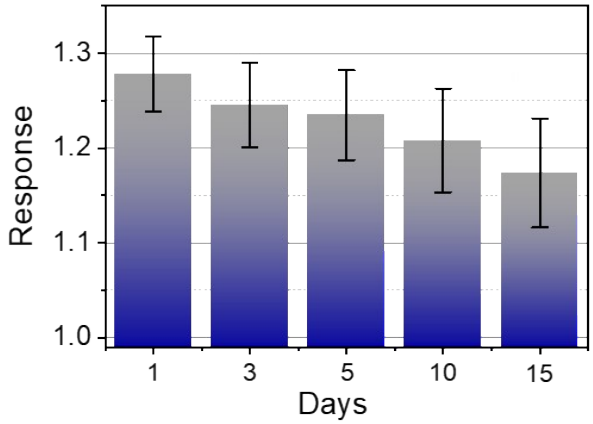

Fig. S16. Stability of the antibody-based biosensors.

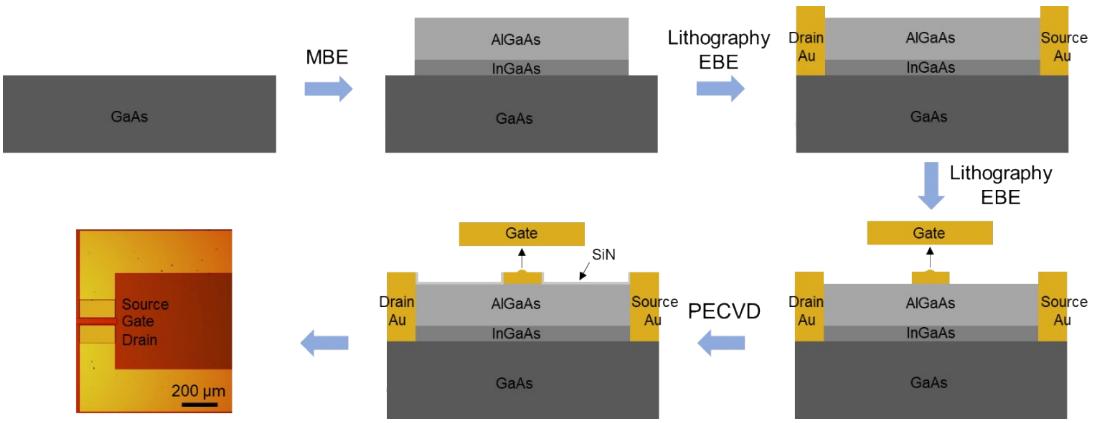

Fig. S17. Preparation processes of HEMT biosensor chip.

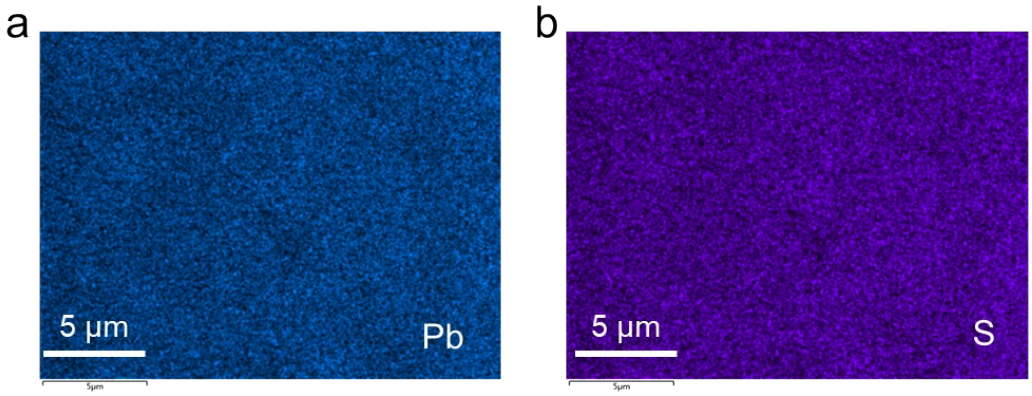

Fig. S18. (a-b) The EDS spectra of CQDs modification layer on the biosensor chip.

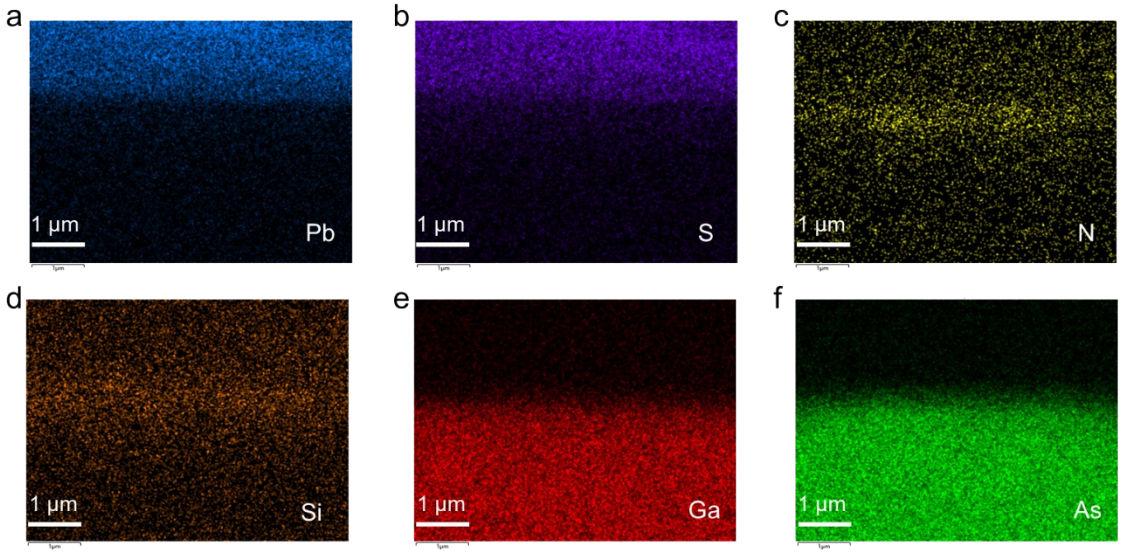

Fig. S19. (a-f)The EDS spectra of CQDs/LCB modification layer on the HEMT device.

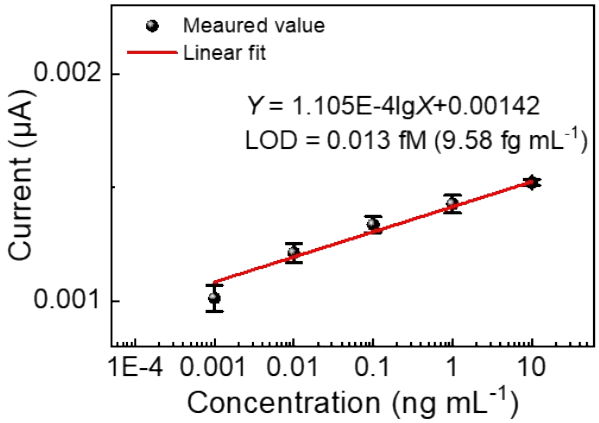

Fig. S20. The current values corresponding to increasing spike protein concentrations.

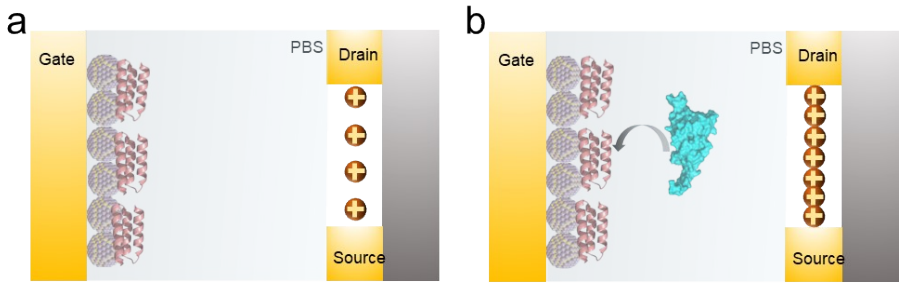

Fig. S21. The analysis lab of biomolecule interactions based on HEMT biosensor chip.

Table S1. Comparison of the reported SARS-CoV-2 spike protein biosensors.

Modified material	ROD	LOD	Solution	Ref.
CE/PbS CQDs/LCB **Au gate/PbS CQDs/LCB**	**10 pg mL^{-1} to 1 µg mL^{-1}** **(13.94 fM to 1394 pM)**	**3.31 pg mL^{-1}** **(4.607 fM)** **9.58 fg mL^{-1}** **(0.013 fM)**	**PBS**	**This work**
CE/CNF-AuNP -chitosan/thiol-terminal aptamer	0.01 to 64 nM	7.0 pM	PBS (phosphate-buffered saline), 5 mM $Fe(CN)_6^{3-/4-}$, 0.1 M	41
Graphene electrode/aluminum oxide/Si-SH-AuNPs/ thiolated aptamer	2.5 to 40.0 ng mL^{-1}	0.8 ng mL^{-1}	PBS containing 1.0 mM $Fe(CN)_6^{4-}$	42
CE/AuNPs/ thiol-functionalized aptamer	10 pM to 25 nM	66 pg mL^{-1}	PBS + 150 mM NaCl + 2 mM $MgCl_2$	43
Au/thiolated H1 (oligonucleotides)	50 fg mL^{-1} to 50 ng mL^{-1}	9.79 fg mL^{-1}	100 mM Diethanolamine buffer containing 1 $mg{\cdot}mL^{-1}$ 1-naphthyl phosphate	44
Monolayer Au/ peptides	0.05 to 10 µg mL^{-1}	0.1 µg mL^{-1}	PBS + 0.05% tween20	45
Au/ortho-phenylenediamine/ SARS-CoV-2-RBD template molecules	2.5 to 40.0 pg mL^{-1}	0.7 ng mL^{-1}	50.0 µL of saliva sample was mixed with 50.0 µL of PBS	46
CE/rGO/EDC-NHS /S1 antibody	2.5 to 40 µg mL^{-1}	150 ng mL^{-1}	PBS solution having 0.1 M of KCl and 5.0 mm of $Fe(CN)_6]^{3-/4-}$	47
Graphitic carbon/EDC-NHS/ethylenediamine (EDA)/anti-SARS-CoV-2 antibody	0.2 to 100 ng mL^{-1}	25 pg mL^{-1}	$[Fe(CN)_6]^{3-/4-}$ in PBS	48
CE/Pd-Au nanosheets/S1 protein antibody	0.01 to 1000 ng mL^{-1}	7.2 pg mL^{-1}	5 mM $[Fe(CN)_6]^{3-/4-}$ solution in PBS	49
Pt/polypyrrole (Ppy) with SARS-CoV-2-S spike glycoprotein	5 to 25 µg mL^{-1}	-	PBS	50
Au/PbS CQDs/Anti-SARS-CoV-2 antibody	50 to 2500 ng mL^{-1}	4.99 ng mL^{-1}	PBS	26